# Analysis of the fatigue life of metal composites with a layer of zirconium alloy

*Szymon Derda*[1*], *Aleksander Karolczuk*[1], *Grzegorz Robak*[1], and *Mariusz Prażmowski*[1]

[1] Faculty of Mechanical Engineering, Opole University of Technology, Mikołajczyka 5, 45-271 Opole, Poland

**Abstract.** Methods of joining dissimilar materials gain interest and attention of highly demanding branches of modern engineering. Acquiring high-quality bond between steel and titanium or zirconium alloys is perceived as especially advantageous in terms of high strength and corrosion resistance. In the present paper results of fatigue tests performed on five different metal composites produced in the process of explosive welding has been gathered. All tested materials were manufactured by a collision of zirconium flyer plates with base plates made of steel or steel-titanium bimetal. Fatigue tests have been conducted under uniaxial force-controlled tension-compression conditions with a constant amplitude of load applied parallelly to bonding interface. The analysis includes the residual stresses measured by the hole-drilling strain gauge method in the flyer plates and the applied stresses calculated by three different models. A description of the initiation and propagation of cracks developing within the joint during cyclically changing loading is also included. Based on the collected data, application conclusions were formulated regarding the optimal use of the tested materials.

## 1 Introduction

Unconventional methods of joining materials are becoming more and more popular due to the increasing demand for modern structures' performance. Making a permanent connection between materials with significantly different properties is desirable because of the unsurpassed performance and the possibility of reducing production costs. From the point of view of the power production and chemical industries, it is necessary to provide a structure resistant to corrosive environments with high strength. In the case of the military and aviation industries, it may be advantageous to obtain maximum strength parameters with the lowest possible density. In many cases, a thin layer of reactive material applied to the base material, whose task is to transfer the loads, turns out to be sufficient to achieve parameters that allow operation in a corrosive environment and allows to reduce costs [1,2]. Materials ideally suited to withstand demanding working conditions used for plating are titanium, niobium or zirconium alloys. The latter is of particular interest to the nuclear industry due to its ability to absorb the thermal neutron and resistance against corrosion at high temperature [3,4]. This results in the wide application of zirconium in the production of fuel rods and in the

* Corresponding author: szymon.derda@doktorant.po.edu.pl

construction of the reactor core [5]. One of the solutions to meet this ever-increasing need for material improvement is the production of layer materials using the explosive welding process [6,7]. This technology offers great opportunities, however, it is associated with several characteristic phenomena, the effects of which may turn out to be undesirable. Basic description of the idea behind explosion welding is that chemical explosion can be used to accelerate one of the components to very high velocity [6-8]. During collision at high velocity, the severe material deformation, high temperature gradients and phase changes occur and leave a trace in the material in form of shrinkage cracks [9,10], adiabatic shear bands [11,12] and residual stress [13-15] . Additionally, the connection may turn out to be a stress concentration site [18], which in the case of cyclically changing loading will affect the service life of the material. Increasing the level of knowledge about the material is crucial for conscious and safe construction and operation.

The aim of the presented paper is to identify the residual stresses and fatigue properties of zirconium coated metal composites produced in the process of explosion welding.

## 2 Experiments

### 2.1 Tested materials

All tested materials were produced in the process of explosive welding in a parallel system using explosives, the main component of which was ammonium nitrate. The base material of the plates was steel. Steel grade varied among the Cases. All of them contained a flyer layer made of Zr 700 zirconium alloy. Three plates were made with the use of an interlayer to ensure the improvement of the quality of the joint used in the case of large differences in properties of the joined materials. Table 1. contains parameters on the joining process, such as: initial distance $\delta$, detonation velocity $v_D$, thickness $t$ and type of individual layers.

**Table 1.** Parameters of explosion welding process

| Case | Flyer | $t$, mm | Interlayer | $t$, mm | Base | $t$, mm | Detonation velocity, $v_D$, mm | Stand-off distance $\delta$, mm |
|---|---|---|---|---|---|---|---|---|
| 1 | Zr 700 | 10 | Ti Gr. 1 | 2.0 | SA516 Gr 60 | 14 | 2500 | 10 (flyer $\delta$ Ti/SA516) |
| 2 | Zr 700 | 10 | Ti Gr. 1 | 2.0 | SA516 Gr 60 | 14 | 2500 | 15 (flyer $\delta$ Ti/SA516) |
| 3 | Zr 700 | 10 | Zr 700 | 3.5 | SA516 Gr 60 | 25 | 3000 | 6+25 (flyer $\delta$ Ti $\delta$ SA516)* |
| 4 | Zr 700 | 3.5 | - | - | SA516 Gr 70 | 20 | 2500 | 3 |
| 5 | Zr 700 | 3.5 | - | - | 10CrMo9-10 | 18 | 2500 | 9 |

$t$ – thickness, * single welding process

Summary of the mechanical properties of the constituent materials including Young's modulus $E$, Poisson ratio ν, yield point $R_{p02}$, tensile strength $R_m$ and elongation $A$ is presented in Table 2.

**Table 2**. Mechanical properties of materials used in explosion welding

| Material | $E$, GPa | ν, - | $R_{p02}/R_{eH}$, MPa | $R_m$, MPa | $A$, % |
|---|---|---|---|---|---|
| Zr 700* | 101 | 0.37 | 216 ($R_{p02}$) | 269 | 35 |
| Ti Gr. 1* | 109 | 0.36 | 251 ($R_{p02}$) | 325 | 46 |
| SA516 Gr 60* | 193 | 0.30 | 268 ($R_{p02}$) | 391 | 41 |
| SA516 Gr 70** | 200 | 0.30 | 371 ($R_{eH}$) | 532 | 31 |
| 10CrMo9-10** | 200 | 0.29 | 447 ($R_{eH}$) | 568 | 26 |

* tested, ** supplier certificates

In the process of joining, five variants of layered metal composites were obtained:

**Case 1.** 14 mm layer of SA516 Gr 60 steel was used as a base layer in the first explosive welding to bond with a 2 mm layer of Ti Gr. 1 titanium alloy (a technological interlayer). The bimetal was covered with a 10 mm layer of Zr 700 zirconium alloy. The final process was carried out with the standoff distance of the joined plates equal to 10 mm.

**Case 2.** Material identical to that described in Case 1. with the difference in the final standoff distance of the plates equal to 15 mm. This difference translated into a higher collision velocity corresponding to a longer standoff distance.

**Case 3**. Three plates joined in one explosion welding process. 25 mm layer of SA516 Gr 60, 3.5 mm interlayer made of Ti Gr. 1 and 10 mm layer made of Zr 700. The distance between the individual layers was 6 and 25 mm, respectively.

**Case 4**. A 3.5 mm thick Zr 700 flyer plate was joined to a base plate of 20 mm thick Sa516 Gr 70 high strength boiler steel. No technological interlayer was used in the process. The standoff distance between the plates was 3 mm.

**Case 5.** A 3.5 mm thick Zr 700 flyer plate connected to a base plate of 18 mm thick 10CrMo9-10 high strength low-alloy boiler steel. No technological interlayer was used in the process. The standoff distance between the plates was 9 mm.

For each case microscopic observations of the interface were carried out. It allowed to gather crucial information about the bond and specify values of characteristic properties. All of them are presented in Table 3 ($H$ – interfacial wave height and *EMT* - equivalent melted thickness, description could be found in [14]).

**Table 3.** Wave height and *EMT* value based on microscopic observations

| Case | Interface | Wave height* $H, \mu m$ | Interface | Wave height* $H, \mu m$ | $EMT, \mu m$ |
|---|---|---|---|---|---|
| 1 | Zr 700/ Ti Gr. 1 | 206±38 | Ti Gr. 1/ SA516 Gr 60 | 71±27 | 3.2 |
| 2 | Zr 700/ Ti Gr. 1 | 236±27 | Ti Gr. 1/ SA516 Gr 60 | 67±23 | 5.1 |
| 3 | Zr 700/ Zr 700 | Undetectable | Zr 700/ SA516 Gr 60 | 343±67 | 73.3 |
| 4 | Zr 700/ SA516 Gr 70 | 122±28 | - | - | 12.6 |
| 5 | Zr 700/ 10CrMo9-10 | 276±73 | - | - | 13.5 |

* - Mean value ± standard deviation

## 2.2 Fatigue tests with interface observation

Fatigue tests were carried out under uniaxial fully reversed cyclic loading set parallel to the bond interface of the composites. Constant force amplitude was varying with the frequency between 1-10 Hz depending on the loading value. The geometry of specimens with different layer orientation were used depending on the number of layers (Fig. 1). Layers thicknesses ($t_1$, $t_2$) and other characteristic sizes (T, w) necessary for stress calculation were measured by optical microscope. Complete separation of a specimen was set as failure criterion of the test.

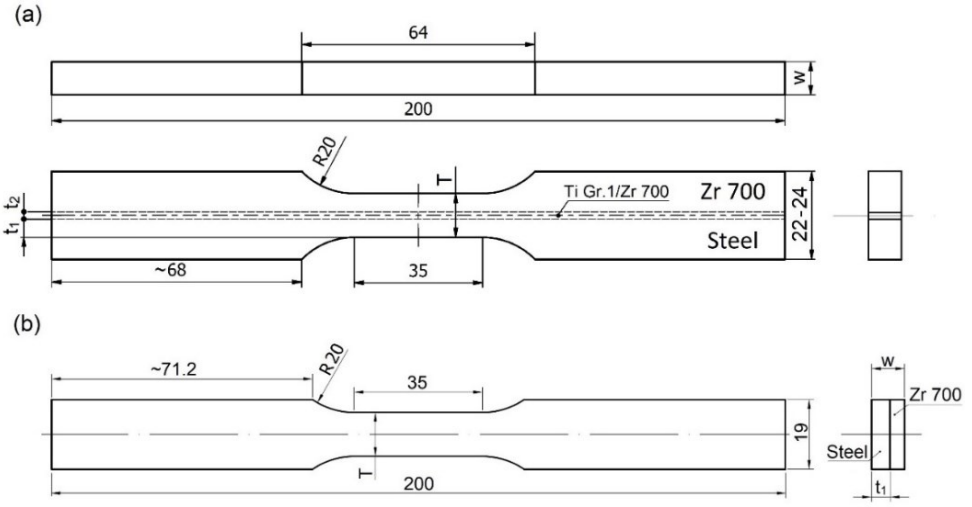


**Fig. 1**. Geometry of the specimen used for fatigue test: a) three layer materials ($T \approx 12.0$ mm, $w \approx 9.0$ mm and $t_1 \approx 4.6$ mm, $t_2 \approx 2.0$ mm for Ti Gr 1 interlayer, and $t_1 \approx 4.2$ mm, $t_2 \approx 3.5$ mm for Zr 700 interlayer), b) two layer materials ($t_1 \approx 5.5$ mm, $T \approx 12.0$ mm, $w \approx 9.0$ mm)

## 2.3 Residual stress

Residual stress state in the flyer layer of Zr 700 was determined using hole drilling strain gauge method (measurement thickness = 1 mm). The method used is the standard test method [16] to determine residual stresses based on stress relaxation induced by the hole-drilling process. Identified plane stress state described by principal stresses is presented in the Figure 2. Several measurements were executed for each Case of the composite. Referential values represent residual stress state in Zr 700 plate used for cladding before explosion welding.

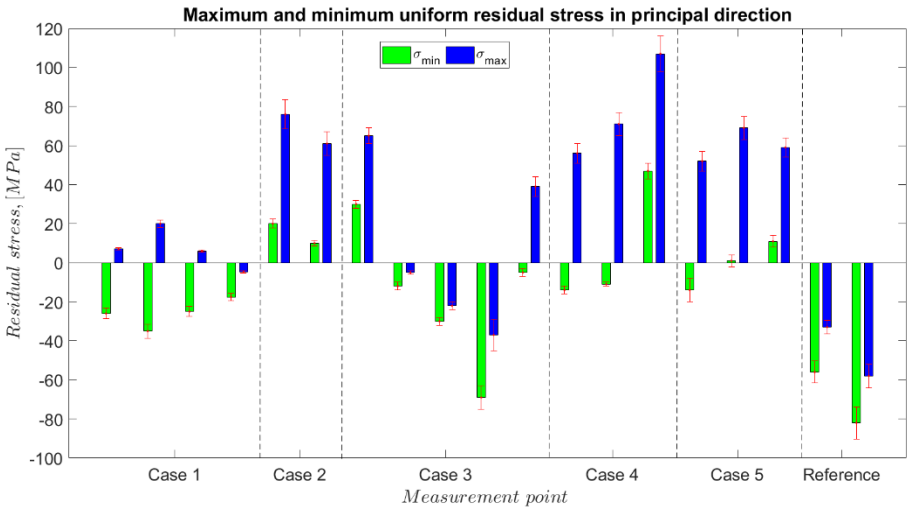


**Fig. 2**. Residual stress state on the surface of Zr 700 layer

## 2.4 Stress calculation

The stresses in each layer were calculated using three models. The first one (analytical) is based on strong assumptions but with the advantage of using without numerical calculation. The second and the third models required finite element analysis. They differ in geometrical modelling of bonding interface. The models assume that all material layers are made of isotropic material and deformed under elastic strain range with the elastic properties presented in table 2.

The first (analytical) approach to stress calculation in each layer is based on several assumptions. Some of them, such as uniform strain distribution along the cross-section, arise from the loading condition - the specimen is attached in the grips of fatigue machine. Assumptions of continuous flat plane of connection between layers, uniaxial stress state and linear elastic strain range allow to express following force balance equation:

$$\Sigma_{i=1}^{3} E^{(i)} A^{(i)} \varepsilon_a - F_a = 0. \tag{1}$$

Considering example of three layer material force balance equation takes form:

$$A^{(1)} E^{(1)} \varepsilon_a + E^{(2)} A^{(2)} \varepsilon_a + E^{(3)} A^{(3)} \varepsilon_a - F_a = 0, \tag{2}$$

where $\varepsilon_a$ is strain amplitude, $E$ is Young's modulus, $A$ is cross-sectional area, $F_a$ is force amplitude and index *(i)* corresponds to *i*-th layer of the material. As a consequence, stress amplitude $\sigma_a$ in each layer can be represented in the following form, as was also shown in [17, 18]:

$$\sigma_a^{(i)} = \frac{F_a E^{(i)}}{\Sigma_{i=1}^{3} E^{(i)} A^{(i)}}. \tag{3}$$

In order to deepen the understanding of how the stress distribution is influenced by wavy-shaped geometry of connection between layers a simple 2D static simulation was performed using ANSYS software. Firstly, the model which corresponds with actual loading conditions of the specimen with flat interface was prepared as shown in Figure 3. Next, a submodeling technique was implemented to use displacement field from the first step as boundary

conditions which were interpolated to nodes of new models – sections of a measurement segment. One with flat line and another with wavy line of connection between layers. Both with considerably increased amount of elements compared to previous step in order to ensure reliable results.

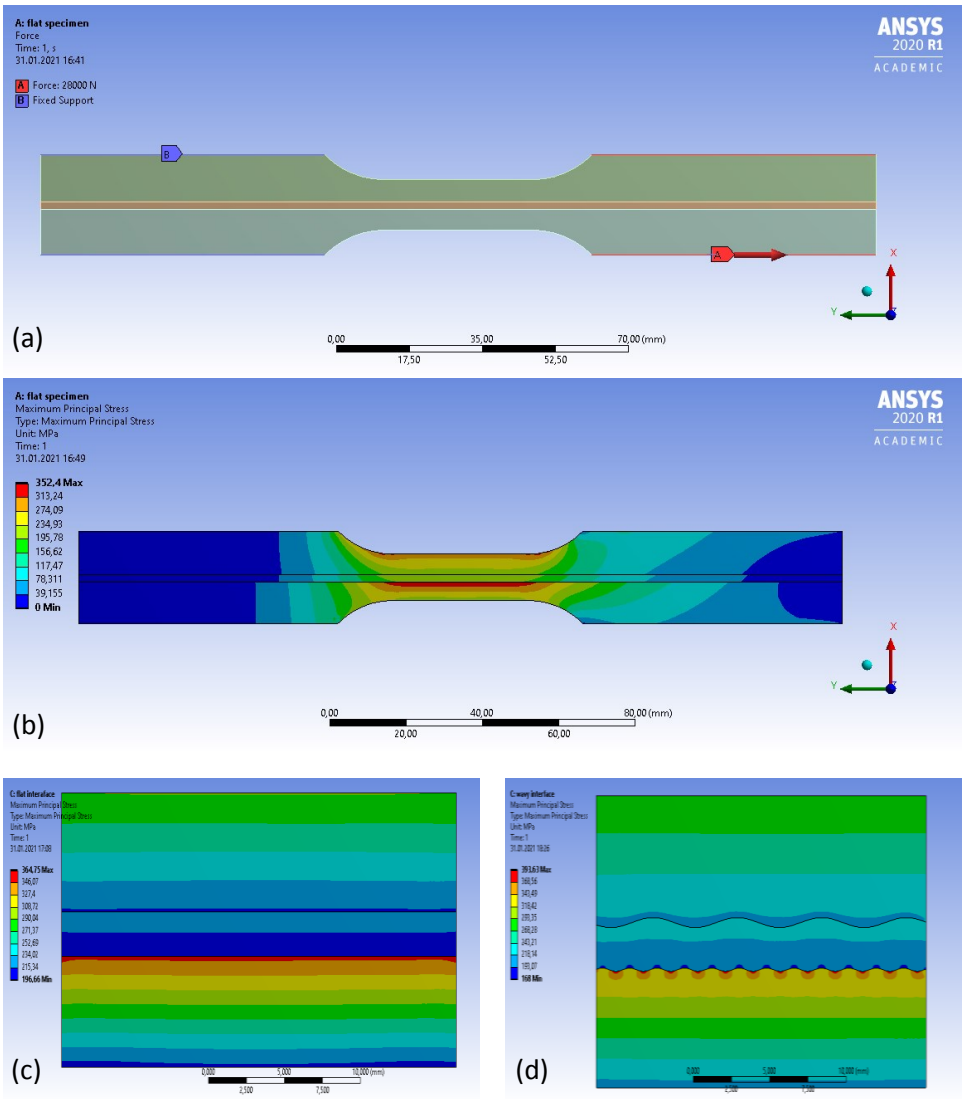


**Fig. 3**. Ansys simulation steps : a) specimen geometry with flat interface, b) results of the initial simulation, c) detailed results of the submodel with flat interfaces, d) detailed results of the submodel with wavy interfaces

A comparison between results obtained using different methods for Case 1 specimen is presented in Figure 4. FEM models tend to give more detailed information on how stress is distributed within a specimen. Maximum principal stress for a specific Case 1 specimen loaded with force $F_a$ = 28 kN calculated using analytical method (eq. 2) was equal to $\sigma_{max}^{analitycal}$=353 MPa. FEM model with flat interface gave very similar results. The highest stress level was located at the interface between P265GH steel and Ti. Grade 1 and was equal

to $\sigma_{max}^{FEM-flat}$=365 MPa. The simulation has shown that the change in geometry of the interface towards more accurate, wavy form based on the identified characteristics of the bond, increases maximum principal stress. In this case it was equal to $\sigma_{max}^{FEM-wavy}$=394 MPa.

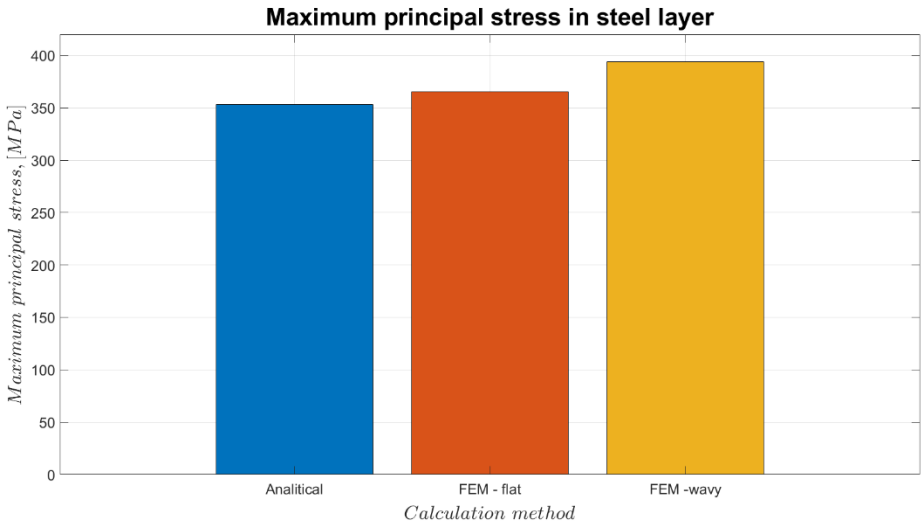


**Fig. 4**. Example of maximum principal stress in steel layer based on the Case 1 specimen

## 3 Results and discussion

The negative principal residual stresses detected in Zr700 plate in state before welding was partially transformed into tensile character (Fig. 2) as result of explosive welding process. The highest tensile residual stress was observed for Case 4 (the bimetallic plate). Clear correlation between welding parameters and residual stresses was not found.

For the applied elastic material parameters and simulated interface geometries (Case 1, Fig. 3), the effect of wavy interface increased the highest principal stress value approximately by 10% comparing to the analytical calculation with flat interface.

The relations between the experimental fatigue lives $N_{exp}$ and analytically calculated stress amplitudes in steel layer were plotted in Figure 5. Basquin S-N curves were estimated and included. Similarities in experimental data regarding Cases 1 and 2 suggest that the difference in standoff distance during explosion welding did not result in major fatigue performance. Even though the effect is visible in average wave height at the interfaces, EMT value and residual stress state in the outer layer of Zr 700. Micro fatigue cracks were found for these Cases which propagated from melted area of Ti-steel interface but the cracks did not expand enough to cause final fracture (primary cracks leading to fracture were initiated in steel plate). Case 3 is the only example among three layer composites which do not contain Ti Gr. 1 interlayer and is characterized by significantly greater stand-off distance than other Cases. This resulted in higher collision velocity, considerably greater wave height and EMT value. Multiple cracks initiated at the interface were detected and they developed with increasing number of cycles leading to plate failure (Figs. 6 and 7). Cases 4 and 5 are two layer composites. Two major differences between them are base material and standoff distance. Case 5 material was produced with high-strength steel and for stress values around 300 MPa and upwards the fatigue results are similar to that obtained by Cases 1 and 2. For

lower stress values the fatigue life is shorter than for those cases. Crack development observed at the interface in case of Case 4 composite did not lead to final failure of the material. Crack growth was observed between 40 and 50 thousand cycles but then the critical fatigue crack was initiated at the surface of steel layer leading to final fracture. In contrary, for the Case 5, the primary fatigue cracks were initiated at the interface.

The positive residual stresses found in outer surface of Zr700 plates did not affect the fatigue live of two and three layers composites. The fatigue life of testes composites is determined by existence of melted areas at the interface with steel and fatigue strength of steel plate. The highest fatigue strength among the analysed composites was exhibited by three layer plate labelled as Case 1.

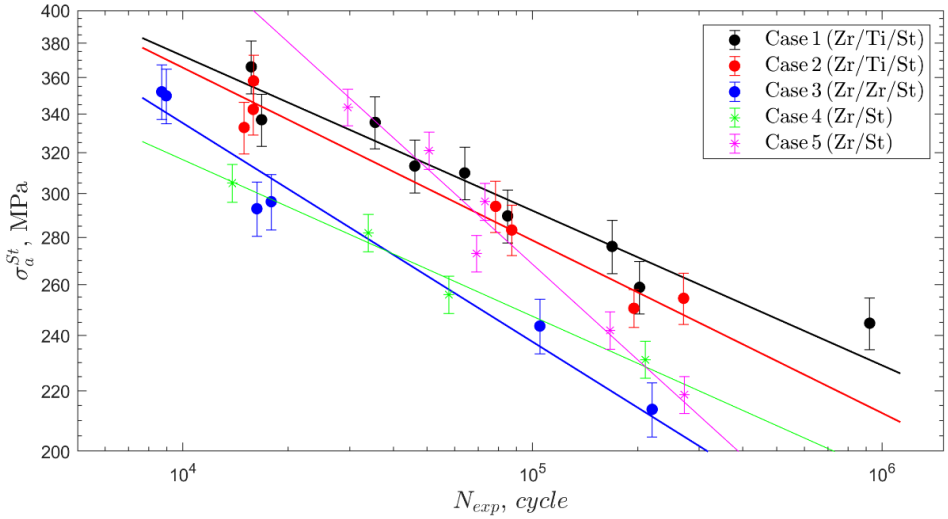


**Fig. 5**. Stress amplitudes in steel as a function of the fatigue life of the tested composites

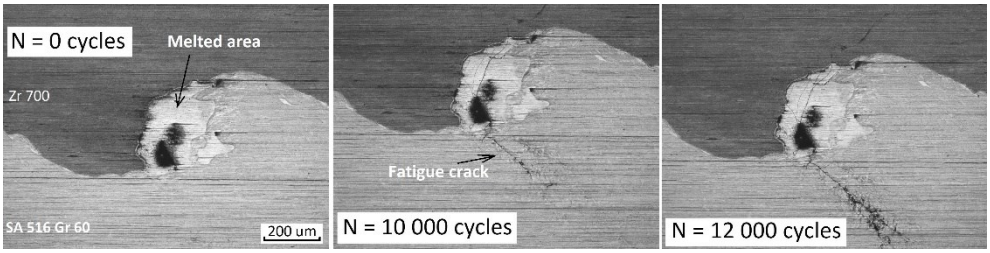


**Fig. 6.** Example of the fatigue crack initiated in the interface for Case 3 and its growth

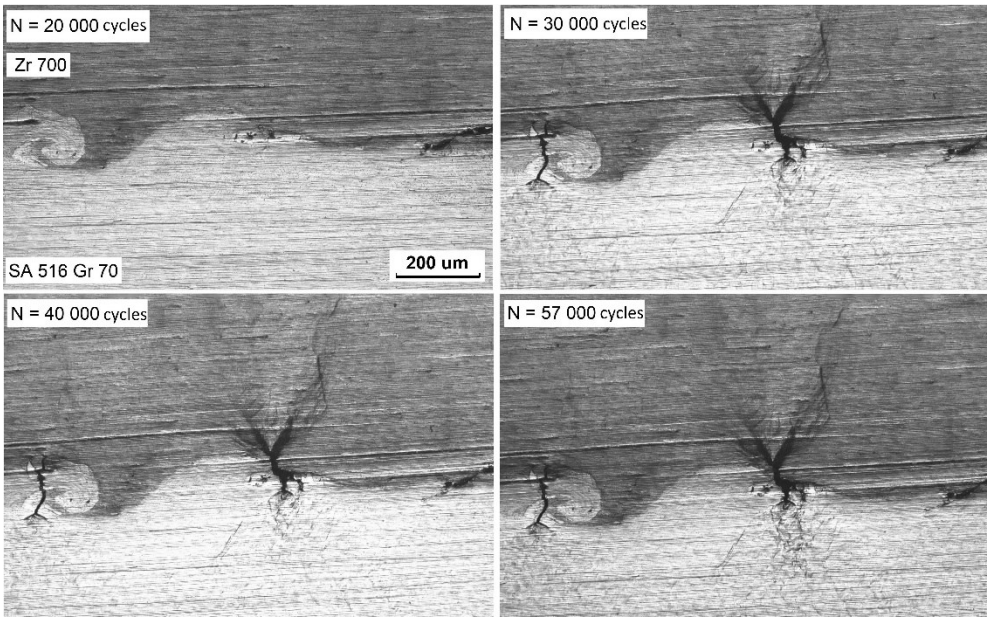


**Fig. 7**. Example of the fatigue cracks initiated in the interface for Case 4 and their growth

## 4 Conclusions

The main conclusions of the study can be summarised in several following points:

- Considerable mechanical properties mismatch and parameters of explosion welding process influence fatigue behaviour of the produced composites.
- Due to irregularities, the complicated geometry of the bond, and other stress concentrating elements such as melted areas, the cracks may initiate in the vicinity of the interface but not necessarily lead to final fracture.
- When the difference in mechanical properties between adjacent layers is insignificant with no melted areas, the fatigue cracks at such interfaces were not found, e.g. Zr 700 – Zr 700 or Zr 700 – Ti Gr. 1 interfaces.
- Among three layer composites Case 3 turned out to be the least favourable in terms of fatigue life.
- Even though the Case 5 material consisted of high strength steel it did not project onto fatigue performance of the composite. As a result its fatigue life was comparable or worse than composites labelled as Cases 1 and 2.

This study was supported by the National Centre for Research and Development, Poland [grant number Techmastrateg2/412341/8/NCBR/2019].

## References

1. J. Banker, J ASTM Int. **7**:1–10 (2010)
2. R. Saranarayanan, AK. Lakshminarayanan, B. Venkatraman, Arch Civ Mech Eng., **19**:251–67 (2019)
3. T. Alam, M. K. Khan, M. Pathak, K. Ravi, R. Singh, S. K. Gupta, Nucl Eng Des, **241**:3658–77 (2011)
4. D. O. Northwood, Mater Des, **6**:58–70 (1985)
5. V. Kalavathi, R. K. Bhuyan, Materials Today: Proceedings **19,** 781–786 (2019)
6. F. Findik, Mater Des, **32**:1081–1093 (2011)
7. B. Crossland, Clarendon Press (1982)
8. M. Prażmowski, M. Najwer, H. Paul, D. Andrzejewski, MATEC Web of Conferences **94**:02012 (2017)
9. T. N. Prasanthi, Sudha, C. Ravikirana, S. Saroja, Mater Des, **93**:180–193 (2016)
10. J. Ning, L. Zhang,M. X. Xie,H.X. Yang,X.Q. Yin,J. X. Zhang, J Alloys Compd, **698**:835–851 (2017)
11. M. Wachowski, M. Gloc, T. Ślęzak, T. Płociński, K. J. Kurzydłowski, J Mater Eng Perform, **26**:945–954 (2017)
12. Y. Yang, B. F. Wang, B. Hu, K. Hu, Z. G. Li, Mater Sci Eng A, **398**:291–296 (2005)
13. A. Karolczuk, M. Kowalski, K. Kluger, F. Żok, Archives of metallurgy and materials, **59**:1119-1123 (2014)
14. A. Karolczuk, K. Kluger, S. Derda, M. Prażmowski, H. Paul, Materials (Basel), **13**:1–14. (2020)
15. A. Karolczuk, K. Kluger, M. Kowalski, F. Żok, G. Robak, Mater Sci Forum, **726**:125–132 (2012)
16. ASTM E837-13a, (2013)
17. A. Karolczuk, A. Carpinteri, G. Robak, S. Derda, M. Prażmowski, Arch Civ Mech Eng, **20**:1–13 (2020)
18. A. Karolczuk, M. Kowalski, R. Bański, F.Żok, Int J Fatigue, **48**:101–8 (2013)